Aswan University Journal of Sciences and Technology Volume 5, issue 3, September 2025

Evaluation of how attenuation correction influences image quality in myocardial perfusion SPECT/CT applying Flash3D iterative reconstruction techniques

Ahmed M. Naguib[a]*, Haroun A. EL sheikh[a], SH. ELmaghraby[b], and Magdy M. Khalil[c]

[a]Department of Physics, Faculty of Science, Aswan University, Aswan 81528, Egypt
[b]Department of Nuclear Medicine and Oncology, Kasr Al-Ainy Hospital, Cairo University, Cairo11421, Egypt.
[c]Department of Physics, Helwan University, Helwan109, Cairo11421, Egypt.

Abstract

This study evaluated Computed tomography (CT) based attenuation correction (AC) in myocardial perfusion imaging (MPI) SPECT/CT using 45 patients (28 males: (mean age: 54.7±12.6 years, mean weight: 79.75±28.2 kg/m²); 17 females: (mean age: 54.8±11.3 years, mean weight: 80.76±28.23 kg/m²)). Participants were categorized by body mass index (BMI), with image quality assessed through the signal-to-noise ratio (SNR) and contrast-to-noise ratio (CNR) metrics using Flash3D reconstruction. Results demonstrated that AC significantly enhanced image quality compared to non-attenuation-corrected (NAC) images. The correction notably reduced false-positive findings caused by diaphragmatic attenuation in male patients and breast tissue attenuation in female patients. Additionally, AC effectively minimized artifactual defects in the inferior and anterior myocardial walls. These improvements highlight the clinical value of CT-based AC in hybrid SPECT/CT systems, as it enhances diagnostic accuracy by addressing gender-specific attenuation challenges. The findings support routine application of AC in MPI protocols to optimize perfusion assessment and reduce interpretation errors related to soft tissue attenuation.

Keywords: Myocardial perfusion imaging; Computed tomography; SPECT/CT; Attenuation correction; Flash3D

1. Introduction

For many years, the noninvasive assessment of coronary artery disease, whether it be suspected or confirmed, has relied heavily on nuclear medicine **[1]**. With the advent of single-photon emission computed tomography (SPECT), myocardial perfusion measurements have improved **[2, 3]**. Scintigraphy offers anatomical, physiological, and functional details. This procedure is a noninvasive technique for assessing how coronary artery disease (CAD) affects cardiac muscle perfusion.

Gated SPECT represents an established modality for assessing ventricular wall motion and calculating ejection fraction. However, the diagnostic accuracy of myocardial perfusion SPECT remains limited by attenuation artifacts, which distort image interpretation. The technique utilizes radioisotopes emitting photons within the 70-360 keV energy range, with tissue interactions primarily governed by two physical phenomena: Compton scattering and photoelectric absorption. These attenuation mechanisms significantly influence image quality by altering photon detection and spatial distribution.

*Corresponding author E-mail: ahmednageb134@yahoo.com
Received July 16, 2025, received in revised form, August 13, 2025, accepted August 13, 2025.

(ASWJST 2021/ printed ISSN: 2735-3087 and on-line ISSN: 2735-3095) https://journals.aswu.edu.eg/stjournal

Attenuation artifacts typically manifest as consistent defects because the positioning of soft tissues relative to the Heart remains unchanged between rest and stress phases of imaging. In women, these artifacts often arise from breast tissue, appearing in the anterior wall of the Heart. At the same time, in men, the diaphragm is a common source, leading to artifacts in the inferior wall **[4]**. The partial volume effect may also distort quantitative measurements for structures smaller than roughly three times the system's spatial resolution.

For a more accurate correction of non-uniform attenuation, computed tomography (CT) has been used. The introduction of integrated SPECT/CT systems due to technological developments in cardiac perfusion imaging has improved diagnostic capacities for physicians. This integration, which Lang, Hasegawa, and associates started, included integrating CT and SPECT hardware and creating AC algorithms with CT data **[5]**.

To increase the accuracy of nuclear cardiology diagnostics, AC procedures are being recommended more and more in current clinical guidelines **[6, 7]**. By considering photon attenuation via biological tissues, these techniques seek to recreate the actual radiotracer dispersion. Based on tissue thickness, composition, and photon energy properties, the physical attenuation process exhibits an exponential connection, as explained by:

$$I = I_0 \, e^{\sum_i -x_i \mu_i} \qquad (1)$$

where x_i indicates tissue thickness, I and I_0 represent transmitted and starting photon intensity, respectively, and μ_i is the linear attenuation coefficient for each kind of tissue along the photon path. The total of $\sum_i$ represents the overall attenuation throughout all areas, as the index i represents several tissue-type sections along the journey.

For myocardial perfusion SPECT, computed tomography-based attenuation correction (CT-AC) has become the gold standard among the several AC techniques. CT-AC performs better than traditional methods with reduced acquisition times, increased photon flux detection, and the removal of the need for a radioactive transmission source **[8, 9]**. In actual practice, these technological benefits result in better image quality and increased diagnostic confidence, especially for myocardial perfusion measurement.

An attenuation map (AM) needs to be created before CT-AC may be used in MPI. The spatial distribution of linear attenuation coefficients (ACO) within the scanned field that corresponds to different anatomical locations is depicted in this map **[6, 10]**. In areas where tissue-related signal loss has previously occurred, the AM is crucial for restoring photon count density and adjusting for photon attenuation. These coefficients, which are customized to each patient's unique anatomical makeup, measure the percentage of photon energy absorbed or dispersed per unit thickness of biological tissue. The accuracy and resolution of the CT-derived AM are crucial for high-quality cardiac imaging. A thorough grasp of the physical concepts, imaging procedures, and hardware involved in the CT-SPECT integration process is necessary to achieve precise image registration and spot possible inconsistencies during acquisition and reconstruction.

This work examines the clinical effects of CT-AC on the qualitative evaluation of myocardial perfusion using SPECT-MPI, with an emphasis on the enhancements in picture quality and diagnostic advantages.

2. Materials and methods

All patients provided their explicit consent for the data to be used. Forty-five patients with probable coronary artery disease (CAD) who had technetium-99m-methoxyisobutylisonitrile (Tc99m-sestamibi) SPECT (selective computed tomography) were included in the study sample. After excluding patients with other cardiac disorders, these patients exhibited normal blood flow and left ventricular function. They also did not have established coronary artery disease.

2.1. Study population

Patients with suspected coronary artery disease (CAD) who were referred for technetium-99m methoxyisobutylisonitrile (Tc-99m sestamibi) SPECT -MPI with CT-AC were included in this prospective study, which was carried out at the Department of Nuclear Medicine, Aswan Oncology Center, Aswan, Egypt. Forty-five patients in all were recruited and divided into two groups according to their BMI and gender. Of the 28 male patients in Group A, 10 were obese (BMI ≥ 30 kg/m^2) and 18 were non-obese (BMI < 30 kg/m^2). Based on the same BMI criterion, 12 of the 17 female patients in Group B were obese and 5 were non-obese. Every subject went through the normal MPI procedures. On a dedicated processing workstation, the Flash3D iterative reconstruction algorithm was used to reconstruct both NAC and AC images.

To be eligible, participants had to be free of a documented history of CAD and have normal left ventricular function and myocardial perfusion. The study excluded patients who had undergone coronary artery bypass grafting, percutaneous coronary intervention, or myocardial infarction before stress imaging. This study aimed to evaluate myocardial perfusion imaging quantitatively and emphasize how crucial precise co-registration between CT and SPECT images is for the best possible diagnostic quality.

2.2. Stress/Rest protocol

Technetium-99m sestamibi is advised for myocardial perfusion imaging following the International Commission on Radiological Protection's guidelines. Patients were instructed to fast for four hours before testing and to avoid caffeine-containing foods and beverages, such as tea, coffee, and chocolate-based drinks, for at least twelve hours. Long-acting nitrates were stopped for 12 hours before the test, beta-blockers were stopped 72 hours before, and calcium channel blockers were stopped 48–72 hours before. Before imaging operations, intravenous access was obtained, and each patient received a baseline physical examination and electrocardiogram (ECG) **[11]**. The modified Bruce protocol, which started with two preliminary phases at 2.7 km/h with 0% and 5% inclines, was used to conduct an exercise stress test on patients who could engage in physical activity. The standard Bruce protocol was then implemented **[12]**. When ischemia ECG modifications appeared or the heart rate reached 85% of the anticipated maximal heart rate, the test was terminated.

The radiotracer was administered intravenously at peak stress, followed by 60 seconds of exercise to enhance myocardial uptake. For patients unable to undergo physical stress testing, pharmacologic stress was induced using dipyridamole **[13]**. These individuals were instructed to avoid methylxanthine-containing substances, such as caffeine, for at least 24 hours before testing. Dipyridamole was infused at a dose of 0.56 mg/kg over 4 minutes. The radiotracer was injected

between 3 and 5 minutes after the completion of the infusion. Throughout the procedure, continuous blood pressure, heart rate, and electrocardiogram (ECG) were monitored to ensure patient safety and assess physiological responses **[14]**.

A two-day imaging protocol was employed, which is considered superior to a single-day protocol due to its ability to reduce cumulative radiation exposure and minimize residual activity (shine-through) from the initial radiotracer injection. The stress-phase injection consisted of 333–555 MBq of Tc-99m, corresponding to an effective dose of approximately 2.3–3.8 mSv. The same radiotracer activity and dose range were used during the rest-phase imaging on the second day **[15]**.

2.3. Acquisition parameters

The gamma camera rotates around the patient, acquiring multiple static images from different angles. These images, known as projections, are formed by detecting photons emitted from the radiotracer within the body. Unlike planar X-rays, which present overlapping anatomical and functional data in a single view, SPECT projections offer depth and localization of radiotracer distribution, despite some photon scatter throughout the body **[16]**. When a multi-detector CT (MDCT) system is placed adjacent to the SPECT unit, the patient can be seamlessly transferred into the SPECT scanner via a table extension, facilitating efficient hybrid imaging.

2.3.1 CT data acquisition

In AC imaging, the SPECT scan is preceded by a CT acquisition. The CT component used in this study was a *SIEMENS SOMATOM* scanner equipped with the Syngo CT workplace (Somaris/5 syngo CT). Cross-sectional transmission images are obtained using a high-powered X-ray tube and a fixed array of detectors arranged in a circular geometry. During image acquisition, the body's tissues preferentially absorb lower-energy photons, resulting in a phenomenon known as beam hardening. This effect reduces the attenuation coefficients for deeper anatomical structures. CT images are calibrated and expressed in Hounsfield Units (HU) to standardize interpretation, allowing for consistent representation of tissue-specific attenuation values **[6]**.

$$HU_{tissue} = \frac{\mu_{tissue}(E_{CT}) - \mu_{W}(E_{CT})}{\mu_{W}(E_{CT})} \times 1000 \qquad (2)$$

In this context, HU_{tissue} represents a given tissue's Hounsfield Unit (HU) value. At the same time, $\mu_{tissue}(E_{CT})$ and $\mu_{w}(E_{CT})$ denote the linear attenuation coefficients for tissue and water, respectively, measured at the effective CT energy, E_{CT}. By definition, CT voxels composed entirely of water are assigned a HU of 0, whereas those containing air are assigned -1000 HU. Therefore, converting HU values into corresponding linear attenuation coefficients is essential for accurate AC. Once derived, these coefficients can be integrated into the image reconstruction process to correct for photon attenuation effects. For reliable correction, attenuation must be accounted for during the iterative reconstruction stage. This study performed a single CT attenuation scan immediately before the SPECT emission scan. The CT acquisition was conducted using a helical scan mode with parameters set to 80 kV tube voltages and 20 mA current. Following acquisition, all imaging data were transferred to a shared processing workstation provided by the manufacturer (*SIEMENS, Health Care*), specifically the *SYNGO MI APPLICATION VB10B* platform.

2.3.2. SPECT data acquisition

All patients underwent Tc-99m MIBI SPECT imaging with CT-AC during stress and rest phases. SPECT acquisitions were initiated immediately following the CT scans using a *SIEMENS SYMBIA* system. The imaging was conducted using a dual-head gamma camera with parallel-hole collimators, arranged in a 90° detector configuration. The SPECT system was calibrated for Tc-99m imaging, and patients were positioned supine with their arms raised above their heads. Data were collected over a noncircular orbit using a step-and-shoot acquisition protocol, beginning at a 45° start angle **[11]**.

Projection data were acquired across a 180° arc, ranging from the right anterior oblique to the left posterior oblique views, with a 3° angular increment. Imaging parameters included a matrix size of 128 × 128 and a pixel resolution of 4.80 mm. Each projection was collected over 25 seconds to evaluate the impact of acquisition time and photon count statistics on overall image quality. The system acquired 32 angular views, each subdivided into 8 frames, effectively capturing the radiation events from multiple angles to support accurate image reconstruction. A 20% symmetric energy window and the 140 keV photo peak were the focal points of image capture during gated acquisition, which used eight frames per R-R interval **[17]**. After acquisition, all imaging data were moved utilizing a Symbia T-2008 workstation to a centralized processing and reconstruction platform offered by *SIEMENS Healthcare (SYNGO MI APPLICATION VB10B)*.

2.4. Reconstruction Steps for converting MPI from non-AC to AC imaging

After the CT scan, the resulting images were transformed into attenuation maps for SPECT using two primary techniques: (1) the use of specific reference points to align CT and SPECT images accurately, and (2) the conversion of CT Hounsfield units into linear attenuation coefficients appropriate for 99mTc photon energies. The CT volume was resampled to correspond with the voxel and pixel dimensions of the SPECT dataset to fuse the CT and SPECT data **[18]** successfully. Because the CT matrix in this study was 512 × 512 and the SPECT acquisition matrix was 128 × 128 pixels, it was necessary to compute the proper scaling factors to balance the two image types during the reconstruction and AC procedures. Multiplying matrix size by pixel size yielded the field of view (FOV): 128 × 4.80 mm = 614.40 mm for SPECT and 512 × 0.78 mm = 399.36 mm for CT. Thus, the scaling factor between the two modalities was 1.53. Following image registration, CT values were linearly converted to attenuation coefficients $\mu\,(j)$ at an effective energy of 80 keV, appropriate for soft tissue, air, water, and bone.

Linear attenuation coefficients were derived from CT Hounsfield units corresponding to the energy level of SPECT emission photons (140 keV). Larsson's calibration curve converted these CT values into attenuation coefficients specific to 99mTc photon emissions **[19]**. This curve provides the necessary conversion factor for accurate AC.:

$$\mu\,(j) = 9.05 \times 10^{-5} HU\,(j) + 0.154 (HU \geq 0)$$

$$\mu\,(j) = 1.54 \times 10^{-4} HU\,(j) + 0.154 (HU < 0)$$

$HU(j)$ refers to the Hounsfield Unit of pixel j at 80 keV, and $\mu(j)$ denotes the corresponding linear attenuation coefficient in cm^{-1}.

A bilinear fitting model established a linear correlation between CT values and tissue attenuation properties. The resulting attenuation maps were subsequently smoothed in all directions.

2.5. Iterative Reconstruction

CT is crucial in SPECT imaging by enabling precise, non-uniform AC. With the development of advanced reconstruction techniques, particularly iterative algorithms, AC has become clinically viable. A key challenge in preprocessing is accurately determining compensation values for each pixel within the projection data.

When AC is applied directly to reconstructed images, the Influence of activity distribution is mitigated; however, challenges persist, especially in media with uniform attenuation. Although correction methods exist for non-uniform attenuation, one of the key drawbacks is noise amplification, particularly in the image's central regions. In contrast, iterative reconstruction techniques are more adept at managing attenuation effects. These algorithms provide a comprehensive mathematical framework that allows for detailed modeling of the physics of emission and detection and associated noise characteristics.

Iterative reconstruction begins with a preliminary image estimate. The algorithm then refines this estimate repeatedly, comparing the calculated projections with the measured data until the discrepancy falls below a defined threshold **[20, 21]**. The process concludes when the simulated projection data sufficiently match the acquired projections. Generally, image resolution improves with an increasing number of iterations; however, excessive iterations may introduce greater image noise. In this study, Flash 3D iterative reconstruction was employed to enhance resolution, with the understanding that beyond a certain point, additional iterations may degrade image quality due to noise.

Flash 3D uses ordered-subset expectation maximization (OSEM), a statistically driven reconstruction method that accounts for distance-dependent blurring effects caused by the collimator in all three spatial dimensions. This physically realistic modeling enhances overall image quality. The algorithm integrates attenuation maps directly into the reconstruction process to produce attenuation-corrected SPECT images.

To reduce image noise post-reconstruction, Flash 3D applies a smoothing filter. The recommended approach involves a matched 3D Gaussian filter with a full-width at half maximum (FWHM) approximately twice the pixel size, or specifically 8.4 mm as suggested by the manufacturer. Siemens' implementation of this high-performance OSEM algorithm is called Flash 3D, as seen in **Figure 1**, which incorporates CT-derived attenuation coefficients during reconstruction to generate corrected images.

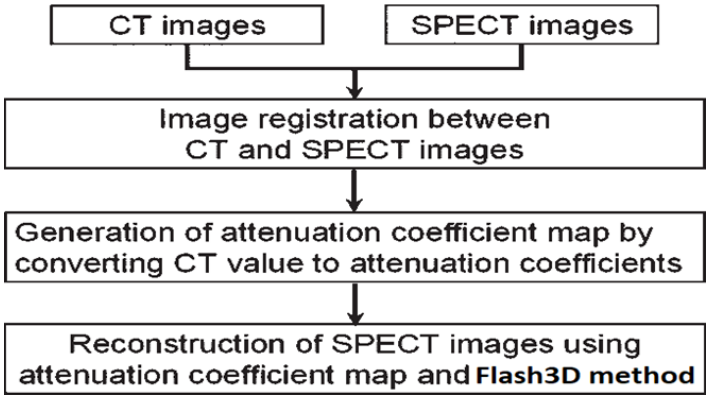

Figure 1: Flowchart shows process in which CT images are used to correct attenuation on SPECT images with Flash 3D reconstruction method **[16]**.

2.6 Quantitative Myocardial Perfusion Imaging

The MPI image quality is determined by statistical data analysis, including the mean count and standard deviation. Several key metrics, including image SNR and CNR, were used to assess the quality of the images. The maximum count of circumferential profiles was used to measure the former two parameters. As a result, the maximum count was utilized for the computations since an oval region of interest (ROI) that covered the whole myocardial slice was drawn across transaxial normal slices.

Figure 2 illustrates how the latter two factors were evaluated using the manufacturer's software and available tools to design a region of interest for the transaxial section with the myocardial cavity as the background.

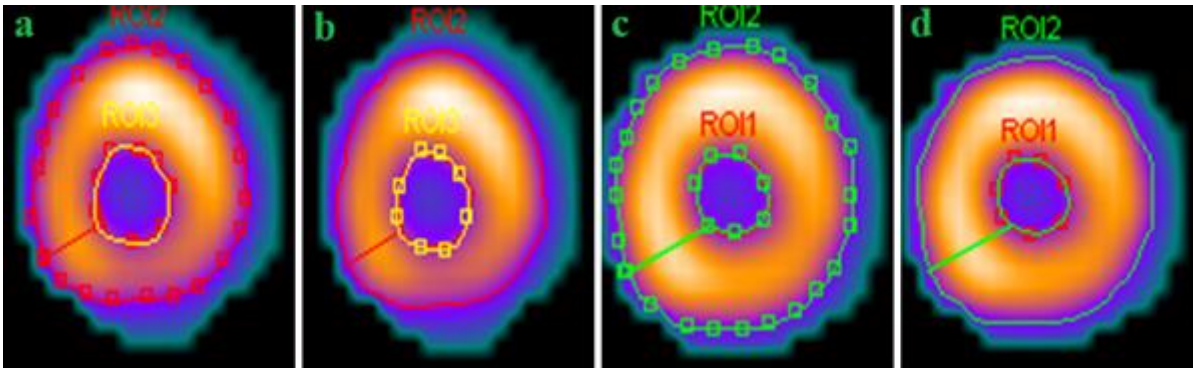

Figure 2. An oval ROI of size covering the whole myocardium slice drawn over trans axial slices: For non-AC (a) measured count at cardial wall and (b) measured count at cardial cavity. For AC (c) measured count at cardial wall and (d) measured count at cardial cavity.

Contrast-to-Noise Ratio (CNR): CNR compares the contrast between an object and its background to the noise level. CNR helps determine the ease of visual differentiation between an object and its surrounding tissue, especially in noisy images.

Signal-to-Noise Ratio (SNR): SNR is the ratio of the strength of a desired signal to the strength of the background noise. SNR measures how much signal is present relative to the noise, indicating the overall quality of a signal or image.

All physical parameters were assessed using short-axis slices of the reconstructed images. The SNR reflects the relationship between the desired signal and background noise; a higher SNR indicates that the signal is more dominant than the noise, thus contributing to clearer and more diagnostically useful images. In contrast, the CNR, while similar to SNR in evaluating image quality, accounts for differences in signal contrast by subtracting the background mean before computing the ratio. This distinction is particularly critical in scenarios where the image may appear to have acceptable signal strength (i.e., high SNR). Still, it lacks adequate contrast due to underlying bias or image fog, resulting in a low CNR.

In this study, both SNR and CNR were employed as key quantitative metrics to assess the image quality of SPECT reconstructions. Regions of interest (ROIs) were delineated: ROIA represented the target myocardial wall region, and ROIB corresponded to the myocardial cavity, as illustrated in **Figure 2**. The formulas used to calculate these parameters were adopted from the literature **[22]**, as follows:

$$SNR = \frac{\text{Mean value (myocardium wall)}}{standerd\ deviation\ of\ cavity} \quad (3)$$

$$CNR = \frac{\text{Mean myocardium} - \text{Mean } cavity}{standerd\ deviation\ of\ cavity} \quad (4)$$

These indices provided objective measures to quantify the improvement in image quality resulting from AC and reconstruction techniques.

3. Results

In non-CTAC myocardial perfusion SPECT images, diaphragmatic attenuation had a pronounced effect on the inferior wall of the myocardium, leading to an apparent reduction in tracer uptake. This reduction, clearly visible in the Flash3D iterative reconstruction images, was particularly evident in the inferior and infero-septal myocardial regions. However, these artifacts were significantly mitigated in the AC images, improving myocardial uniformity and more accurate perfusion assessment. A clear contrast in image quality was observed between the AC and non-AC photos, with the AC reconstructions via Flash3D demonstrating superior image homogeneity. The infero-septal wall reduction is highlighted in **Figure 3**, while the attenuation effect in the inferior wall is further illustrated in **Figure 4 (a and b).**

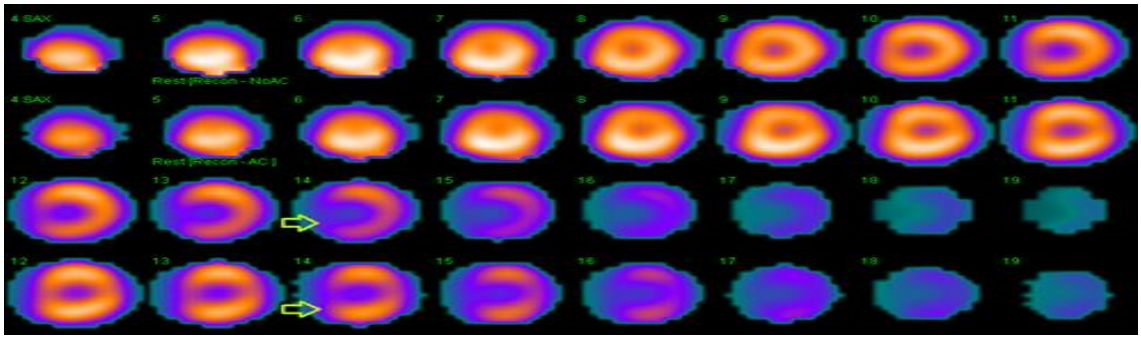

Figure 3: Final attenuation-corrected short-axis cardiac sections obtained with SPECT/CT at a Rest MPI of patient without AC and with AC.

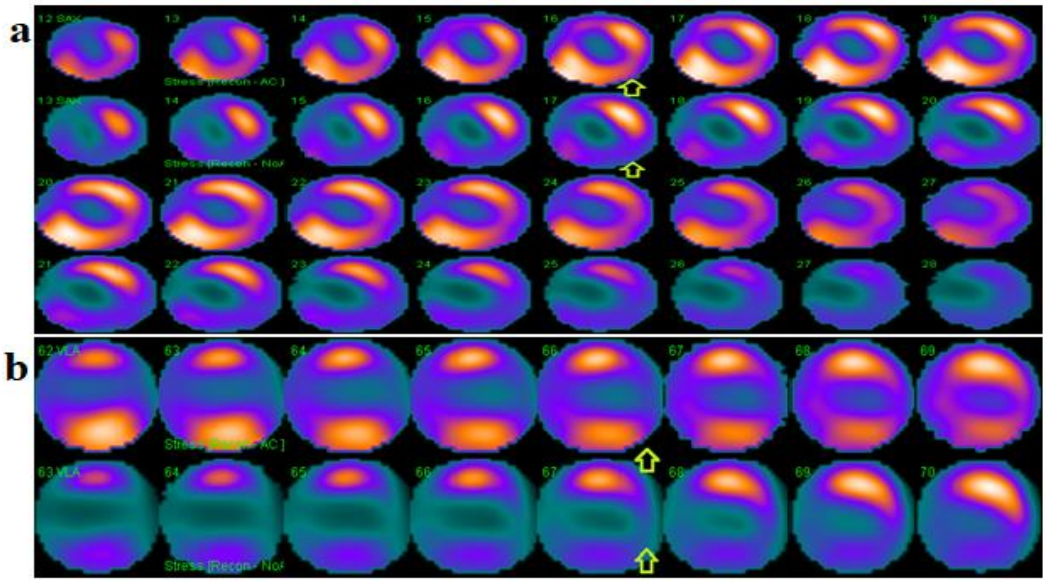

Figure 4: (a) Vertical short axis (VLA) and (b) long axis (SA) slices from myocardial perfusion images of a patient with AC and without AC.

A statistically significant difference was observed in the mean values of SNR and CNR between CTAC and Non-CTAC myocardial perfusion SPECT images. The comparative results of SNR and CNR for the stress-phase MPI are illustrated in **Figures 5 and 6**, while the corresponding values for the rest-phase MPI are presented in **Figures 7 and 8**. A summary of all mean quantitative values is provided in **Tables 1 and 2**.

Figures 5 and 6 compare SNR and CNR for Stress MPI under different conditions: CTAC vs Non-CTAC, across four groups.

Figure 5 shows the average SNR at stress MPI: Female (non-obese) shows the highest SNR with CTAC. Male (non-obese) shows the lowest SNR without CTAC.

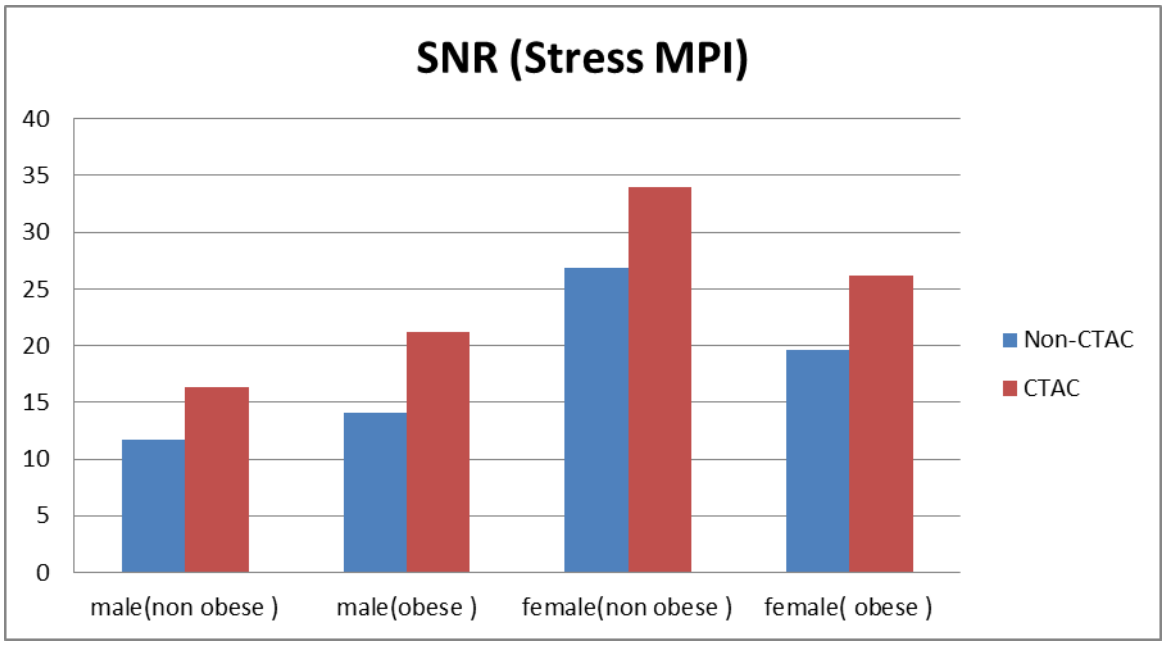

Figure 5: Graph of average of Non-CTAC and CTAC using the Flash3D reconstruction at SNR Stress MPI.

Figure 6 shows the average CNR at stress MPI: The Highest CNR is observed in males (non-obese) under CTAC. Females (non-obese) have the lowest CNR without CTAC.

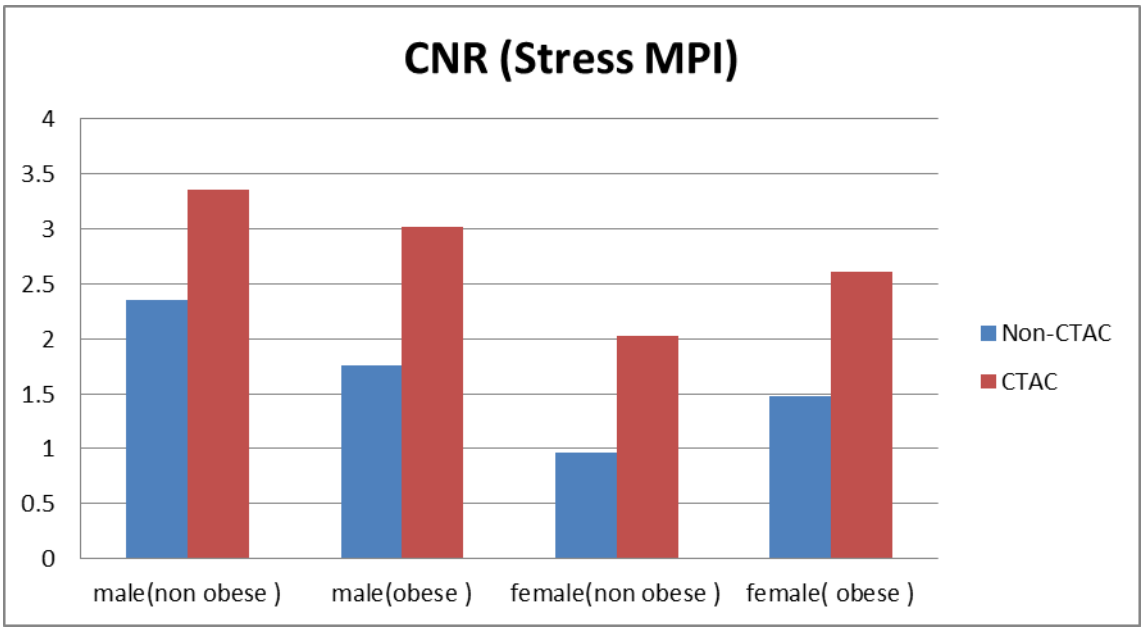

Figure 6: Graph of average of Non-CTAC and CTAC using the Flash3D reconstruction at CNR Stress MPI.

Table 1: Percentages average of Non-AC and AC distributed according to BMI during Stress MPI for SNR andCNR.

Body mass index (BMI)		Stress			
		SNR		CNR	
		Non-CTAC	CTAC	Non-CTAC	CTAC
Male	male BMI values < 30 kg/ m²	11.73694	16.359783	2.349302	3.35969797
	male with BMI values ≥ 30 kg/m²	14.0577	21.2031	1.75784	3.01924595
Female	female BMI values < 30 kg/ m²	26.79608	33.958386	0.967353	2.02861217
	female with BMI values ≥ 30 kg/m²	19.62507	26.1664	1.473631	2.61104134

AC Stress dataset comparing Non-AC vs. AC measurements: AC significantly improved both image quality metrics in stress studies. The mean of SNR increased from 18.054 without AC to 24.421 with AC (mean difference 3.18, p-value <0.0001). The mean of CNR demonstrated greater relative improvement, rising from 1.637 to 2.754, representing a 59.44% increase (p-value <0.0001).

Figures 7 and 8 compare SNR and CNR for Rest MPI under different conditions: CTAC vs Non-CTAC, across four groups.

Figure 7 shows the average SNR at stress MPI: Female (non-obese) shows the highest SNR with CTAC. Male (non-obese) shows the lowest SNR without CTAC.

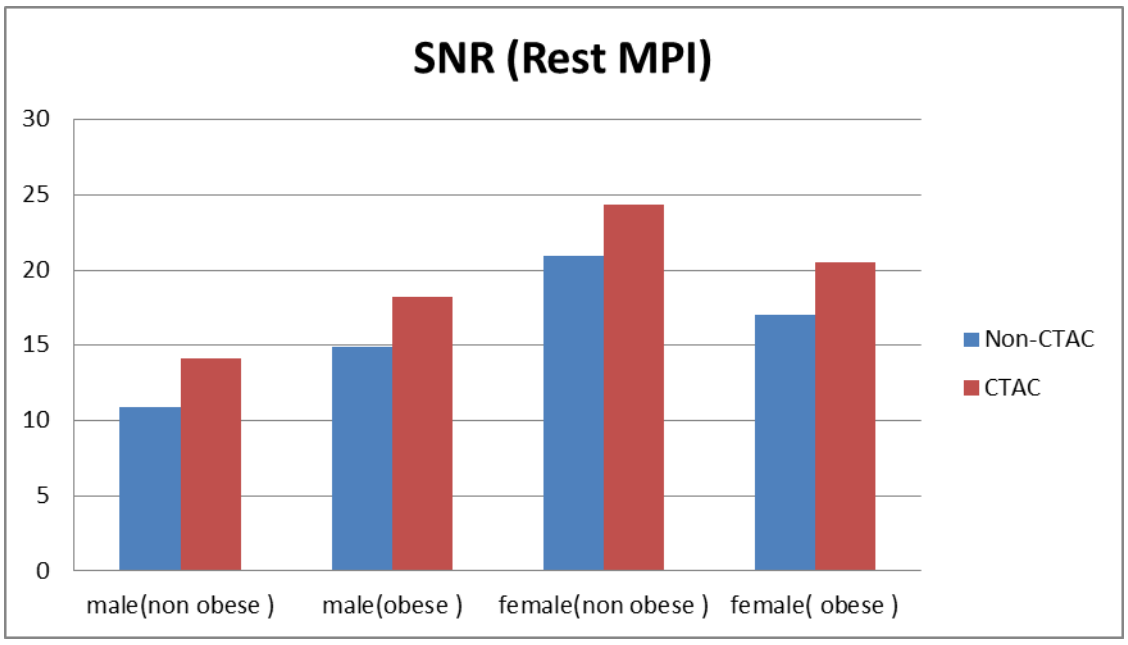

Figure 7: Graph of average of Non-CTAC and CTAC using the Flash3D reconstruction at SNR Rest MPI.

Figure 8 shows the average CNR at stress MPI: The Highest CNR is observed in males (non-obese) under CTAC. Female (obese) has the lowest CNR without CTAC.

CTAC significantly enhances CNR and SNR in Stress and Rest MPI across all groups, with females and obese patients showing the greatest benefit. This supports the routine use of AC in clinical MPI imaging to optimize image quality and diagnostic accuracy.

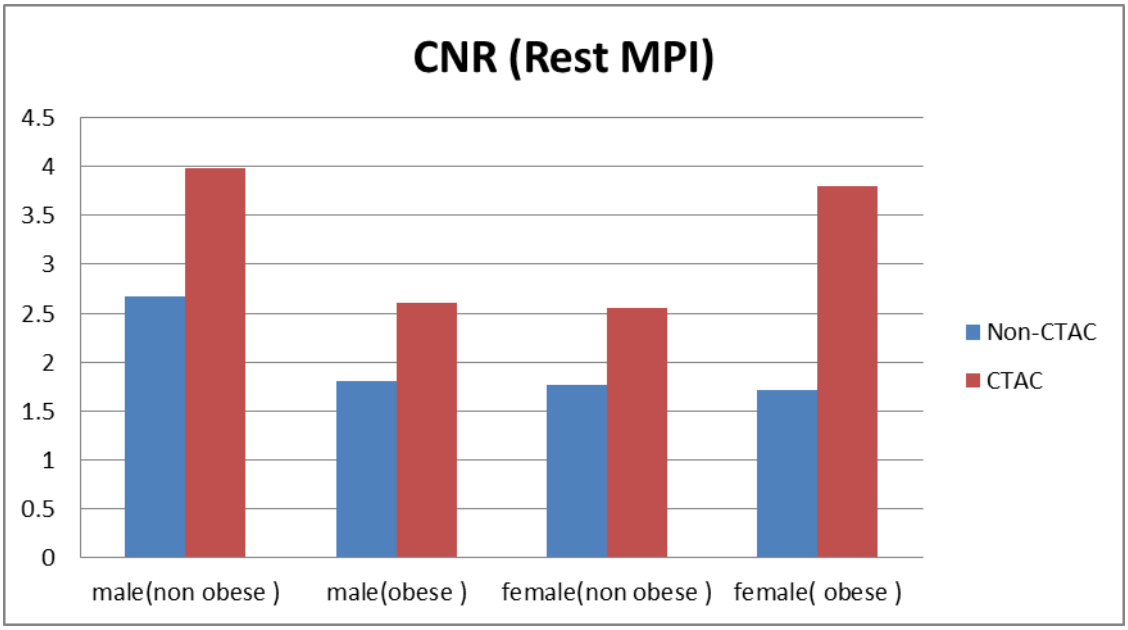

Figure 8: Graph of average of Non-CTAC and CTAC using the Flash3D reconstruction at CNR Rest MPI.

Table 2: Percentages average of Non-AC and AC distributed according to BMI during Rest MPI for SNR and CNR.

Body mass index (BMI)		Rest			
		SNR		CNR	
		Non-CTAC	CTAC	Non-CTAC	CTAC
Male	male BMI values < 30 kg/ m^2	10.89681536	14.17054	2.676845762	3.98025
	male with BMI values ≥ 30 kg/m^2	14.91381989	18.18305	1.807266405	2.60146
Female	female BMI values < 30 kg/ m^2	20.98184932	24.33928	1.763520603	2.55465
	female with BMI values ≥ 30 kg/m^2	17.05696846	20.52105	1.718866237	3.80334

AC Rest dataset comparing Non-AC vs. AC measurements: AC significantly improved both image quality metrics in rest studies. The mean of SNR increased from 15.962 without AC to 19.303 with AC (mean difference 1.67, p-value <0.0001). The mean of CNR demonstrated greater relative improvement, rising from 1.992 to 3.235, representing a 61.57% increase (p-value <0.0001).

4. Discussion

In MPI, soft tissue attenuation artifacts can lead to an increased incidence of false-positive findings and a consequent reduction in the diagnostic specificity of rest and stress scans. The use of iterative reconstruction algorithms combined with AC has been shown to effectively reduce these false-positive results by compensating for photon attenuation caused by overlying anatomical structures and addressing resolution loss due to depth-dependent detector sensitivity and photon scatter. It is well established that cardiac SPECT imaging's attenuation patterns differ between sexes. Specifically, women are more prone to attenuation artifacts in the anterior wall due to breast tissue. In contrast, men commonly exhibit attenuation effects in the inferior wall, primarily resulting from the diaphragm **[23]**.

The principle underlying photon attenuation in SPECT imaging suggests that the likelihood of a photon traversing tissue diminishes as the path length through the attenuating medium increases. This explains why pixels closer to dense attenuating structures exhibit more pronounced attenuation effects. While photon activity does not significantly influence quantitative measurements, it appears to impact qualitative image interpretation. The findings indicate that AC is more effective in the presence of substantial attenuation (e.g., thick attenuating tissues) or under low-count imaging conditions. Furthermore, precise co-registration between CT and SPECT images is strongly recommended due to the critical role of accurate attenuator representation in correction algorithms **[18]**.

Technetium-99m (Tc-99m) SPECT imaging under rest-stress protocols is widely recognized as a reliable noninvasive diagnostic tool for assessing patients with suspected or confirmed coronary artery disease (CAD). The American Society of Nuclear Cardiology (ASNC) endorses using a low-dose protocol during the stress phase as a standard clinical practice **[24]**. This approach offers several advantages for patient care, including reduced radiation exposure during the rest phase, optimized imaging workflow, and improved procedural efficiency, collectively contributing to cost reduction **[25]**.

Many studies have demonstrated that AC helps both obese and non-obese patients, with the benefit being higher for those with a BMI of ≥30. According to recent research, patients with a BMI of ≥30 had a worse diagnostic accuracy with non-attenuation corrected SPECT [23]. For these patients, AC increased diagnostic accuracy and specificity. Additionally, it has been proposed that AC improves the normality and specificity in non-obese patients **[26]**.

Diagnostic-quality single photon emission computed tomography (SPECT) imaging is feasible in morbidly obese patients using a dual-head camera, AC, and high stress Tc-99m tracer doses. Exercise stress was associated with better image quality. The prognostic value of a normal MPI study in this population appears to be less favorable than in non-morbidly obese patients **[27]**.

MPI in obese individuals presents notable challenges due to increased soft tissue attenuation and the greater distance between the Heart and the detector. These factors, along with limited exercise capacity, suboptimal acoustic windows, and reduced signal-to-noise ratios, can compromise the diagnostic reliability of noninvasive cardiac imaging modalities **[28]**.

Our quantitative assessment demonstrated significant differences in image quality between CTAC and non-CTAC datasets across all patient groups. Specifically, SNR and CNR metrics varied substantially, indicating a notable improvement in radiotracer distribution with the application of CTAC. AC significantly enhances both CNR and SNR in stress and rest MPI , with improvements varying by gender and BMI subgroups. Non-obese males exhibited the greatest gains, while obese females showed more modest but still significant improvements. (AC) significantly improves both CNR and SNR in MPI across all demographic subgroups (p- value <0.0001) **[29, 30]**.

The findings confirm that AC is critical for enhancing image clarity and diagnostic precision. Furthermore, our results suggest that qualitative image quality improves with larger attenuating structures and under conditions of increased radiotracer activity, implying that correction algorithms perform more effectively in these scenarios.

5. Conclusion

In hybrid SPECT/CT imaging, spatial co-registration enables the integration of physiological data from the emission scan with anatomical information derived from the CT transmission scan. This alignment allows the CT component to produce an attenuation map, which serves as the basis for AC in the SPECT data, particularly in quantitative analyses. When the CT images possess adequate spatial resolution and contrast, they can also mitigate partial volume effects, thereby refining the accuracy of SPECT reconstructions.

This study examined the relationship between BMI and image quality in MPI by comparing mean SNR and CNR values in AC and non-AC images reconstructed with the Flash3D algorithm during rest and stress phases. Significant differences in SNR and CNR were observed between obese and non-obese patient groups, indicating that BMI affects MPI image quality. The findings highlight the need for personalized imaging protocols to enhance diagnostic accuracy, especially for obese patients and women, who often pose greater technical challenges in nuclear cardiology. Consistent with previous research **[29, 30]**, the study recommends that AC should be routinely applied in MPI, particularly for non-obese males. For obese and female patients, additional protocol adjustments such as extended acquisition times or dose modifications may be necessary to achieve optimal image quality and accurate diagnostic outcomes.

The growing adoption of SPECT/CT systems in clinical practice is largely attributed to their ability to produce reliable AC through high-quality CT-derived attenuation maps, contributing to more accurate and consistent diagnostic outcomes.

Acknowledgments

The authors express their sincere gratitude to the Aswan Oncology Center and Aswan University's Faculty of Science for their invaluable support and provision of research infrastructure.

Conflict of interest statement

All authors declare that no competing financial interests or personal relationships could influence this work.

Author Contribution

All authors participated equally in study design, execution, analysis, and manuscript preparation and approved the final version.

References

1. Dvorak, R.A.; Brown, R.K.; Corbett, J.R. Interpretation of SPECT/CT Myocardial Perfusion Images: Common Artifacts and Quality Control Techniques. Radiographics 2011, 31, 2041–2057.
2. Ryan, A.; Dvorak, M.R.; James, M.D.; Corbett, R. Interpretation of SPECT/CT Myocardial Perfusion Images: Common Artifacts and Quality Control Techniques. Radiographics 2011, 31, 2041–2057.
3. Dvorak, R.A.; Brown, R.K.; Corbett, J.R. Interpretation of SPECT/CT Myocardial Perfusion Images: Common Artifacts and Quality Control Techniques. Radiographics 2011, 31, 2041–2057.
4. Lang, T.F.; Hasegawa, B.H.; Liew, S.C.; Brown, J.K.; Blankespoor, S.C.; Reilly, S.M.; et al. Description of a Prototype Emission Transmission Computed Tomography Imaging System. J. Nucl. Med. 1992, 33, 1881–1887.

5. LaCroix, K.J.; Tsui, B.M.W.; Hasegawa, B.H.; Brown, J.K. Investigation of the Use of X-ray CT Images for Attenuation Compensation in SPECT. IEEE Trans. Nucl. Sci. 1994, 41, 2793–2799.
6. Patton, J.A.; Turkington, T.G. SPECT/CT Physical Principles and Attenuation Correction. J. Nucl. Med. Technol. 2008, 36, 1. https://doi.org/10.2967/jnmt.107.046839.
7. Stakhiv, O.; Melo, I.; Clarke, M.; Aplin, M.; Singh, N.; Day, K.; et al. Influence of Computed Tomography Attenuation Correction in Myocardial Perfusion Imaging in Obese Patients: Classification by Sex and Body Mass Index. In Proceedings of the 3rd International Conference on Numerical and Symbolic Computation, ECCOMAS, Portugal, 2017; pp. 283–292.
8. Goetze, S.; Brown, T.L.; Lavely, W.C.; Zhang, Z.; Bengel, F.M. Attenuation Correction in Myocardial Perfusion SPECT/CT: Effects of Misregistration and Value of Reregistration. J. Nucl. Med. 2007, 48, 1090–1090.
9. Ou, X.; Jiang, L.; Huang, R.; Li, F.; Zhao, Z.; Li, L. Computed Tomography Attenuation Correction Improves the Risk Stratification Accuracy of Myocardial Perfusion Imaging. Nucl. Med. Commun. 2013, 34, 5.
10. Zaidi, H.; Hasegawa, B. Determination of the Attenuation Map in Emission Tomography. J. Nucl. Med. 2003, 44, 291–291.
11. Anagnostopoulos, M.H.C.; Kelion, A.; Kundley, K.; Loong, C.Y.; Notghi, A.; Reyes, E.; et al. Procedure Guidelines for Radionuclide Myocardial Perfusion Imaging. Heart 2004, 90, i1–i10.
12. Bruce, R.A. Multi-Stage Treadmill Test of Submaximal and Maximal Exercise. In Exercise Testing and Training of Apparently Healthy Individuals: A Handbook for Physicians; The American Heart Association: New York, NY, USA, 1972; pp. 32–34.
13. Wolthuis, R.A.; Froelicher, V.F.; Fischer, J.; Triebwasser, J.H. The Response of Healthy Men to Treadmill Exercise. Circulation 1977, 55, 153–157.
14. Leppo, J.A. Dipyridamole Myocardial Perfusion Imaging. J. Nucl. Med. 1994, 35, 730–733.
15. DePuey, E.G.; Mahmarian, J.J.; Miller, T.D.; Einstein, A.J.; Hansen, C.L.; Holly, T.A.; et al. Patient-Centered Imaging. J. Nucl. Cardiol. 2012, 19, 185–215.
16. Utsunomiya, D.; Nakaura, T.; Honda, T.; Shiraishi, S.; Tomiguchi, S.; Kawanaka, K.; et al. Object-Specific Attenuation Correction at SPECT/CT in Thorax: Optimization of Respiratory Protocol for Image Registration. Radiology 2005, 237, 662–669.
17. Cherry, S.R.; Sorenson, J.A.; Phelps, M.E. Physics in Nuclear Medicine; Saunders: Philadelphia, PA, USA, 2013; pp. 209–211.
18. Meysam, T.; Marian, N. Quantitative Evaluation of the Effect of Attenuation Correction in SPECT Images with CT-Derived Attenuation. In Physics of Medical Imaging, SPIE, 2019; Volume 10948, pp. 1364–1373.
19. Larsson, A. Corrections for Improved Quantitative Accuracy in SPECT and Planar Scintigraphic Imaging; Umeå Universitet: Umeå, Sweden, 2005; p. 88.
20. DePuey, E.G.; Bommireddipalli, S.; Clark, J.; Leykekhman, A.; Thompson, L.B.; Friedman, M. A Comparison of the Image Quality of Full-Time Myocardial Perfusion SPECT vs. Wide Beam Reconstruction Half-Time and Half-Dose SPECT. J. Nucl. Cardiol. 2011, 18, 273–280.
21. Einstein, A.J.; Johnson, L.L.; DeLuca, A.J.; Kontak, A.C.; Groves, D.W.; Stant, J.; et al. Radiation Dose and Prognosis of Ultra-Low-Dose Stress-First Myocardial Perfusion SPECT in Patients with Chest Pain Using a High-Efficiency Camera. J. Nucl. Med. 2015, 56, 545–545.
22. Bormans, G.; van der Hiel, E. Signal-to-Noise Ratio in Medical Imaging: Implications for SPECT and PET. Med. Phys. 2022, 49, 1230–1237.
23. Tamam, M.; Mulazimoglu, M.; Edis, N.; Ozpacaci, T. The Value of Attenuation Correction in Hybrid Cardiac SPECT/CT on Inferior Wall According to Body Mass Index. World J. Nucl. Med. 2016, 15, 18–23.
24. Gibson, P.B.; Demus, D.; Noto, R.; Hudson, W.; Johnson, L.L. Low Event Rate for Stress-Only Perfusion Imaging in Patients Evaluated for Chest Pain. J. Am. Coll. Cardiol. 2002, 39, 999–1004.

25. Holly, T.A.; Abbott, B.G.; Al-Mallah, M.; Calnon, D.A.; Cohen, M.C.; DiFilippo, F.P.; et al. Single Photon-Emission Computed Tomography. J. Nucl. Cardiol. 2010, 17, 941–973. https://doi.org/10.1007/s12350-010-9246-y.
26. Grossman, G.E.; Bateman, T.M.; Heller, G.V.; Johnson, L.L.; Folks, R.D.; et al. Quantitative Tc-99m Sestamibi Attenuation-Corrected SPECT: Development and Multicenter Trial Validation of Myocardial Perfusion Stress Gender-Independent Normal Database in an Obese Population. J. Nucl. Cardiol. 2004, 11, 263–272. https://doi.org/10.1016/j.nuclcard.2004.02.007.
27. Duvall, W.L.; Croft, L.B.; Corriel, J.S.; Einstein, A.J.; Fisher, J.E.; Haynes, P.S.; et al. SPECT Myocardial Perfusion Imaging in Morbidly Obese Patients: Image Quality, Hemodynamic Response to Pharmacologic Stress, and Diagnostic and Prognostic Value. J. Nucl. Cardiol. 2006, 13, 202–209.
28. Duvall, W.L.; Wijetunga, M.N.; Klein, T.M.; Razzouk, L.; Godbold, J.; Croft, L.B.; et al. The Prognosis of a Normal Stress-Only Tc-99m Myocardial Perfusion Imaging Study. J. Nucl. Cardiol. 2010, 17, 370–377.
29. Bormans, G.; van der Hiel, E. Signal-to-Noise Ratio in Medical Imaging: Implications for SPECT and PET. Med. Phys. 2022, 49, 1230–1237.
30. Raza, H.; et al. Comparison of Non-Attenuation Corrected and Attenuation Corrected Myocardial Perfusion SPECT. Egypt. J. Radiol. Nucl. Med. 2016, 47, 783–792.